A Cascaded Coupled Resonator Decoupling Network for Mitigating Interference Between Two Radios in Adjacent Frequency Bands

Luyu Zhao, *Member, IEEE*, Ke-Wei Qian, and Ke-Li Wu, *Fellow, IEEE*

***Abstract*—A new microwave device called the cascaded type of coupled resonator decoupling network (C-CRDN) is proposed in this paper. The four-port device can be used to reduce the interference between two radio systems that work in adjacent or even contiguous frequency bands. A C-CRDN is cascaded between the two antennas to be decoupled and the I/O ports of their radio systems, respectively. The coupling matrix of a C-CRDN can be designed to meet the required isolation and return-loss specifications. To prove the concept, a fourth- and sixth-order C-CRDN using coaxial combline cavities are designed, fabricated, and measured according to the characteristics of a testing array that consists of two high-gain sleeve dipoles working in the adjacent time-division long-term evolution and wireless fidelity bands. The measured results have demonstrated that the proposed C-CRDN can effectively mitigate the coexistence interference between the two collocated systems by providing at least 20-dB isolation improvement and enhanced matching performance. The proposed technique is general and can find many applications in heterogeneous wireless systems.**

***Index Terms*—Co-located transceivers, in-device coexistence (IDC), interference suppression, long-term evolution (LTE), microwave passive network, mutual coupling, wireless fidelity (Wi-Fi).**

I. Introduction

IN ORDER to access various wireless networks and services ubiquitously, there is an irreversible trend in today's heterogeneous wireless communication systems that more and more communication systems of different protocols and working frequencies are integrated into one increasingly compact physical unit. Such a trend impacts not only mobile terminals, but also network infrastructure equipment such as base stations and wireless routers. In a mobile unit, such as a mobile phone or a laptop computer, multiple wireless services, including global system for mobile communication (GSM), Universal Mobile Telecommunications System (UMTS), wireless fidelity (Wi-Fi), long-term evolution (LTE), global navigation satellite system (GNSS) and Bluetooth, coexist in a very compact space. The RF interference among the systems that operate at the same or adjacent frequency bands can seriously affect the quality of service [1], [2]. Meanwhile, in today's wireless base station, antennas for second-generation (2G) (GSM), third-generation (3G) (UMTS), fourth-generation (4G) (LTE), as well as Wi-Fi wireless communication systems must coexist in a close vicinity, which inevitably create RF interference to each other since these frequency bands are very close to each other [3], as shown in Fig. 1.

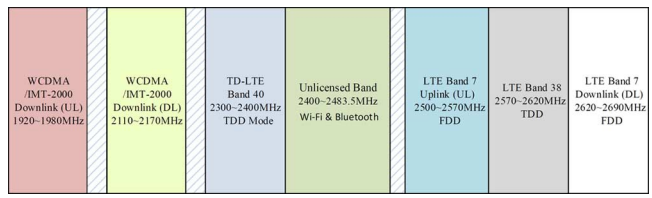

Fig. 1. Available frequency bands within 2–2.7 GHz.

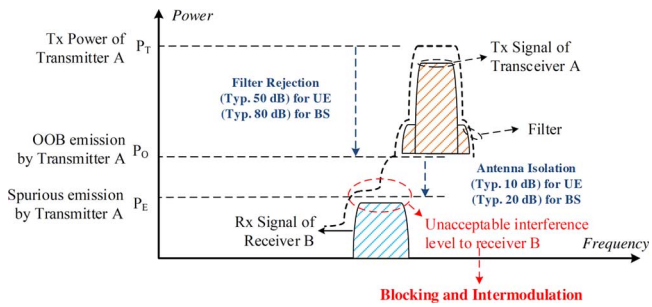

Fig. 2. Coexistence interference from transmitter A to receiver B operating in adjacent frequency bands (user equipment: UE; base station: BS).

A common scenario of the coexistence interference between a transmitter A (TxA) and a receiver B (RxB) is shown in Fig. 2. When the transmitting power of TxA is high or TxA and RxB are in a close proximity in both spatial and spectral senses, the interference from TxA to RxB might be above the noise floor or sensitivity of RxB even with state-of-the-art filter and antenna isolation technologies [1]. The unwanted interference will result in intermodulation and blocking effect [4], which will definitely degrade the performance of the collocated systems.

Although there are many preliminary attempts from industry and academic communities to avoid such interference by adding filters and increasing isolation between two antennas as far as

Manuscript received March 19, 2014; revised July 09, 2014; accepted September 01, 2014. Date of publication September 23, 2014; date of current version November 03, 2014. This work was supported by The Chinese University of Hong Kong under a Postgraduate scholarship. This work was supported in part of the Development and Reform Commission of Shenzhen Municipality under Grant Shen Fa Gai (2013) 1673.

The authors are with the Department of Electronic Engineering and the Shenzhen Engineering Laboratory of Wireless Locating Technology and System, Shenzhen Research Institute, The Chinese University of Hong Kong, Shatin, NT, Hong Kong (e-mail: lyzhao@ee.cuhk.edu.hk; kwqian@ee.cuhk.edu.hk; klwu@ee.cuhk.edu.hk).

Color versions of one or more of the figures in this paper are available online at http://ieeexplore.ieee.org.

Digital Object Identifier 10.1109/TMTT.2014.2358202

possible, the interference among the systems operating at adjacent frequencies cannot be sufficiently suppressed if the spatial isolation is not sufficient. The coexistence interference issue among radio transceivers and antennas becomes increasingly important as the size of an integrated system decreases and the number of wireless systems increases. Current solutions can be divided into three categories, which are: 1) signaling-based solutions that require coordination between the collated transceivers [1], [2]; 2) active interference suppression solutions that need a complex active circuitry and control algorithm [5]–[7]; and 3) antenna isolation enhancement solutions by passive networks [8]–[12]. However, none of them works for the two radio systems working in two unequal frequency bands.

A new breed of microwave passive devices, called the cascaded type of coupled resonator decoupling network (C-CRDN), which can effectively reduce the coupling between two coupled antennas operating at either the same or different frequency bands while providing a good impedance matching, is proposed in this paper. Compared to the existing techniques, the new device has the following unique features:

1) a pure passive network that does not require any electronic circuits nor any power supply;
2) generic and applicable to a wide range of radio interference problems between two uncorrelated radios;
3) providing a controllable additional isolation while providing a good matching bandwidth of the antennas;
4) a filter-like network that allows adoption of many filter design theories and realization technologies [13].

Unlike a conventional microwave filter that is a two-port device, a C-CRDN is a four-port coupled resonator network. Although microwave coupled resonator multiport networks is a popular topic in recent years [14]–[17], most of the developed theories and technologies are concerned with microwave diplexers and multiplexers, which usually possess a common port. Little attention has been paid to decoupling problems of two radio systems. To the best of the authors' knowledge, this work is the first attempt to address this problem. In this paper, the fundamental working principles of the four-port C-CRDN device will be discussed in detail in Section II. Two practical design examples will be given in Section III to demonstrate the effectiveness of the device. The measured results have shown that a C-CRDN can effectively mitigate the coexistence interference between two collocated systems by providing at least 20-dB isolation improvement and enhanced matching performance. The proposed technique is generic and can find many applications in heterogeneous wireless communication systems.

II. C-CRDNs

A C-CRDN device can be very well described by an Nth-order coupled resonator network model with four ports, as shown in Fig. 3(a), from which it can be seen that ports 1 and 2 are connected to the two radio transceivers and ports 3 and 4 of a C-CRDN are connected to the two collocated coupled antennas. The routing diagram of a general ladder coupling topology of the coupled resonators is depicted in Fig. 3(b), where each solid circle represents a microwave resonator resonating at a designed frequency and the solid line and dashed line marked by m_{ij} represent the main line couplings and cross couplings between resonators i and j, respectively. The solid

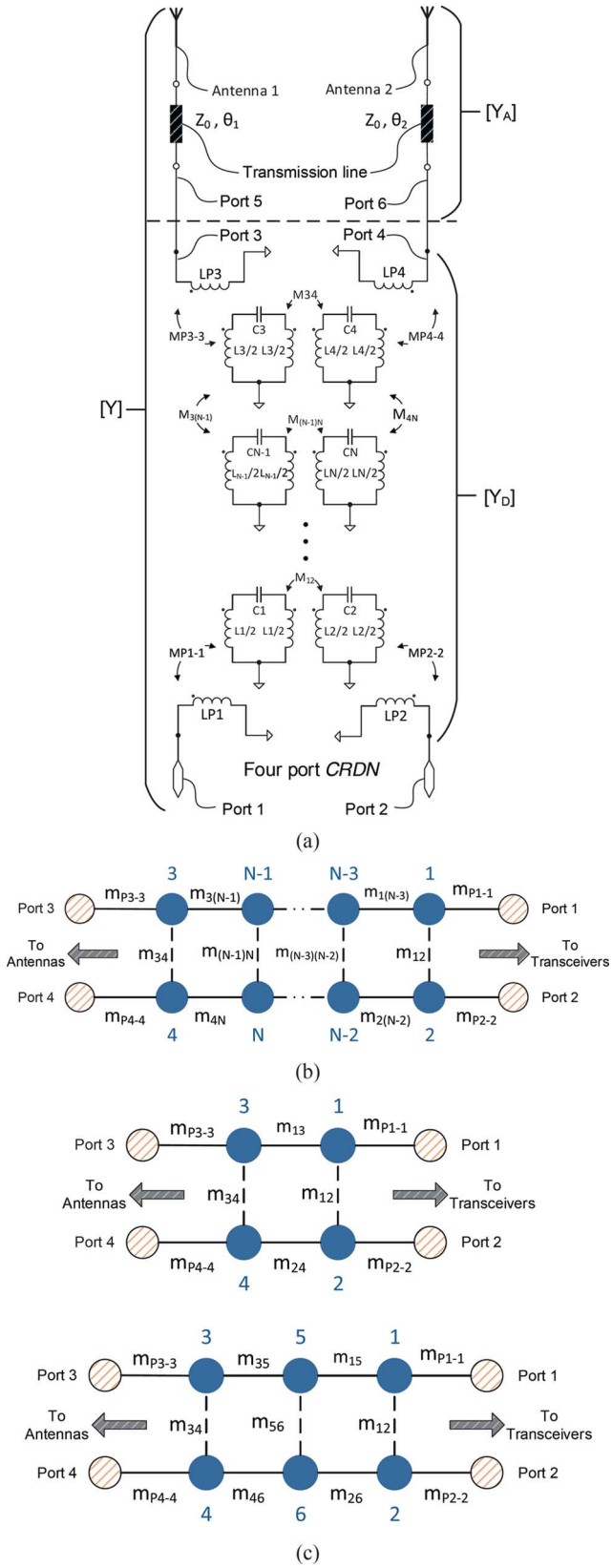

Fig. 3. (a) Circuit model and (b) routing diagram of the four-port Nth-order CRDN. (c) Routing diagrams of a fourth- and sixth-order CRDNs.

line marked by m_{pq-p} represents the coupling between port q and resonator p, which are called I/O couplings.

For two strongly coupled antennas resonating at two adjacent frequency bands, their admittance matrix $[Y^A]$ can be expressed as

$$[\mathbf{Y}^A] = \begin{bmatrix} Y_{11}^A & Y_{12}^A \\ Y_{21}^A & Y_{22}^A \end{bmatrix}. \tag{1}$$

In order to mitigate the coexistence interference caused by the radiating characteristic of the two antennas, a four-port C-CRDN is introduced and is cascaded between the coupled antennas and the transceivers, as shown in Fig. 3(a). The admittance matrix of the C-CRDN, $[Y^D]$, can be written as

$$[\mathbf{Y}^D] = \begin{bmatrix} Y_{11}^D & Y_{12}^D & Y_{13}^D & Y_{14}^D \\ Y_{12}^D & Y_{22}^D & Y_{23}^D & Y_{24}^D \\ Y_{13}^D & Y_{23}^D & Y_{33}^D & Y_{34}^D \\ Y_{14}^D & Y_{24}^D & Y_{34}^D & Y_{44}^D \end{bmatrix}. \tag{2}$$

To find the exact expression of $[Y^D]$ in terms of respective coupling coefficients of the four-port C-CRDN, the circuit model in Fig. 3(a) is investigated. In general, there are N resonant loops with four ports in a C-CRDN. Applying the Kirchoff's voltage law (KVL) and Kirchoff's current law (KCL) to the network schematic, assuming that there are no couplings between the ports, the admittance matrix of the C-CRDN can be expressed as

$$[\mathbf{Y}_D] = j \cdot \left[\overline{\mathbf{M}}_{\mathbf{pr}}(\overline{\mathbf{M}}_{\mathbf{rr}} - j \cdot \overline{\mathbf{S}})^{-1}\overline{\mathbf{M}}_{\mathbf{rp}}\right]^{-1} \tag{3}$$

where

$$\overline{\mathbf{M}}_{\mathbf{pr}} = \begin{bmatrix} m_{p1-1} & 0 & \cdots & 0 & 0 \\ 0 & m_{p2-2} & \cdots & 0 & 0 \\ 0 & 0 & \cdots & m_{p3-(N-1)} & 0 \\ 0 & 0 & \cdots & 0 & m_{p4-N} \end{bmatrix} \in \mathbb{C}^{4\times N} \tag{4a}$$

$$\overline{\mathbf{M}}_{\mathbf{rp}} = \overline{\mathbf{M}}_{\mathbf{pr}}^{\mathbf{T}} \in \mathbb{C}^{N\times 4} \tag{4b}$$

$$\overline{\mathbf{M}}_{\mathbf{rr}} = \begin{bmatrix} m_{11} & m_{12} & \cdots & m_{1N} \\ m_{12} & m_{22} & \cdots & m_{2N} \\ \vdots & \vdots & \ddots & \vdots \\ m_{1N} & m_{2N} & \cdots & m_{NN} \end{bmatrix} \in \mathbb{C}^{N\times N} \tag{4c}$$

$$\overline{\mathbf{S}} = \mathrm{diag}[\mathbf{s}, \mathbf{s}, \ldots, \mathbf{s}] \in \mathbb{C}^{N\times N} \tag{4d}$$

with

$$s = j \cdot \frac{1}{\mathrm{FBW}}\left(\frac{\omega}{\omega_0} - \frac{\omega_0}{\omega}\right) \tag{4e}$$

where ω is the angular frequency in the bandpass domain, $\omega_o L = Z_0$, and the fractional bandwidth (FBW) is a design parameter specified according to the design specification. When a C-CRDN is cascaded to two coupled antennas, the cascaded network becomes a two-port network with its admittance parameter expressed as

$$[\mathbf{Y}] = \begin{bmatrix} Y_{11} & Y_{12} \\ Y_{21} & Y_{22} \end{bmatrix}. \tag{5}$$

To obtain $[Y]$ in terms of $[Y^A]$ and $[Y^D]$, the voltage–current relations of the two coupled antenna network and the C-CRDN are expressed by partitioned matrix representation as

$$\begin{bmatrix} \overline{\mathbf{I}}_1 \\ \overline{\mathbf{I}}_2 \end{bmatrix} = \begin{bmatrix} \overline{\mathbf{Y}}_{11}^D & \overline{\mathbf{Y}}_{12}^D \\ \overline{\mathbf{Y}}_{21}^D & \overline{\mathbf{Y}}_{22}^D \end{bmatrix} \cdot \begin{bmatrix} \overline{\mathbf{V}}_1 \\ \overline{\mathbf{V}}_2 \end{bmatrix} \tag{6}$$

and

$$\overline{\mathbf{I}}_2 = -\overline{\mathbf{Y}}^A \cdot \overline{\mathbf{V}}_2 \tag{7}$$

where

$$\overline{\mathbf{I}}_1 = \begin{bmatrix} I_1 \\ I_2 \end{bmatrix} \quad \overline{\mathbf{I}}_2 = \begin{bmatrix} I_3 \\ I_4 \end{bmatrix} \quad \overline{\mathbf{V}}_1 = \begin{bmatrix} V_1 \\ V_2 \end{bmatrix} \quad \overline{\mathbf{V}}_2 = \begin{bmatrix} V_3 \\ V_4 \end{bmatrix} \tag{8a}$$

are port currents and voltages, respectively, and the sub-matrices are defined as

$$\overline{\mathbf{Y}}_{11}^D = \begin{bmatrix} Y_{11}^D & Y_{12}^D \\ Y_{12}^D & Y_{22}^D \end{bmatrix}$$

$$\overline{\mathbf{Y}}_{12}^D = \begin{bmatrix} Y_{13}^D & Y_{14}^D \\ Y_{23}^D & Y_{24}^D \end{bmatrix}$$

$$\overline{\mathbf{Y}}_{21}^D = \begin{bmatrix} Y_{13}^D & Y_{23}^D \\ Y_{14}^D & Y_{24}^D \end{bmatrix} \tag{8b}$$

$$\overline{\mathbf{Y}}_{22}^D = \begin{bmatrix} Y_{33}^D & Y_{34}^D \\ Y_{34}^D & Y_{44}^D \end{bmatrix}$$

$$\overline{\mathbf{Y}}^A = \begin{bmatrix} Y_{11}^A & Y_{12}^A \\ Y_{12}^A & Y_{22}^A \end{bmatrix}. \tag{8c}$$

The admittances for the cascaded network can then be obtained by substituting (7) into (6),

$$\overline{\mathbf{I}}_1 = [\mathbf{Y}] \cdot \overline{\mathbf{V}}_1 \tag{9a}$$

with

$$[\mathbf{Y}] = \left[\overline{\mathbf{Y}}_{11}^D + \overline{\mathbf{Y}}_{12}^D(-\overline{\mathbf{Y}}^A - \overline{\mathbf{Y}}_{22}^D)^{-1}\overline{\mathbf{Y}}_{21}^D\right]. \tag{9b}$$

Substituting (8) into (9b) yields

$$[\mathbf{Y}] = \begin{bmatrix} Y_{11} & Y_{12} \\ Y_{21} & Y_{22} \end{bmatrix} = \begin{bmatrix} Y_{11}^D & Y_{12}^D \\ Y_{12}^D & Y_{22}^D \end{bmatrix} + \begin{bmatrix} Y_{13}^D & Y_{14}^D \\ Y_{23}^D & Y_{24}^D \end{bmatrix} \cdot \left(- \begin{bmatrix} Y_{11}^A + Y_{33}^D & Y_{12}^A + Y_{34}^D \\ Y_{12}^A + Y_{34}^D & Y_{22}^A + Y_{44}^D \end{bmatrix}^{-1} \right) \cdot \begin{bmatrix} Y_{13}^D & Y_{23}^D \\ Y_{14}^D & Y_{24}^D \end{bmatrix}. \tag{10}$$

Using the S-to-Y transformation, the S_{21} of the cascaded system can be expressed as (by setting $Z_0 = 1$)

$$S_{21} = \frac{-2Y_{21}}{(1+Y_{11})(1+Y_{22}) - Y_{12}Y_{21}}. \tag{11}$$

It is obvious that S_{21} will vanish within a certain band of interest as long as

$$Y_{21}(\omega) \approx 0, \omega \in [\omega_L, \omega_0] \cup [\omega_0, \omega_U] \tag{12}$$

where $\omega \in [\omega_L, \omega_0]$ and $\omega \in [\omega_0, \omega_L]$ are the two adjacent bands of interest.

Having had $Y_{21} \approx 0$, the reflection coefficients at the two ports can be simplified to

$$S_{11} \approx \frac{1 - Y_{11}}{1 + Y_{11}} \quad S_{22} \approx \frac{1 - Y_{22}}{1 + Y_{22}} \tag{13}$$

which means that the two ports in Fig. 3(a) can be independently matched in their respective band of interest if the following constraints on self-admittance parameters are satisfied:

$$Y_{11} \approx 1, \omega \in [\omega_L, \omega_0] \tag{14a}$$

and

$$Y_{22} \approx 1, \omega \in [\omega_0, \omega_U]. \tag{14b}$$

Therefore, the design procedure of a C-CRDN for adjacent frequency bands can be separated into two steps, which are: 1) to design the couplings coefficients of the network such that Y_{21} is minimized and 2) to match the two ports within their respective band of interest. Since $[Y^A]$ in general is frequency dependent, to analytically synthesize $[Y^D]$ is very difficult if not impossible. Therefore, the coupling coefficients of a C-CRDN can be appropriately designed by nonlinear optimization. The overall cost function used in this work is given as

$$K = w_1 \cdot K_{11} + w_2 \cdot K_{22} + w_3 \cdot K_{21} \tag{15a}$$

where

$$K_{11} = \sum_{i=1}^{N_L} |Y_{11}(\omega_i) - 1|^2 \tag{15b}$$

$$K_{22} = \sum_{i=1}^{N_U} |Y_{22}(\omega_i) - 1|^2 \tag{15c}$$

$$K_{21} = \sum_{i=1}^{N_L+N_U} |Y_{21}(\omega_i)|^2 \tag{15d}$$

w_1, w_2, and w_3 are weighting coefficients. N_L and N_U are the numbers of sampling frequency points ω_i selected in the lower and upper frequency bands that are adjacent.

III. Design and Optimization Process

To validate the theory and prove the concept, two high-gain (around 7.6 dBi) sleeve antennas, one of which resonates at 2.35 GHz and the other at 2.45 GHz, respectively, are placed in close proximity to each other as the testing array. Such high gain antennas are used to imitate the characteristic of two high-gain base-station antennas operating in adjacent bands. The 2.35-GHz antennas is assumed to serve the time-division long-term evolution (TD-LTE) band 40, while the 2.45-GHz antenna is assumed for a Wi-Fi system. Such a situation reflects a popular scenario for 4G femto cells where a Wi-Fi router works as a throughput off-load of a TD-LTE wireless system. Fig. 4(a) illustrates the two sleeve antennas, a cascaded C-CRDN, and pre-selection filters for two transceivers. Fig. 4(b) shows the measurement set up of the examples.

Since the TD-LTE band (2300 ~ 2400 MHz) is immediately adjacent to the unlicensed band (2400 ~ 2483.5 MHz) even if

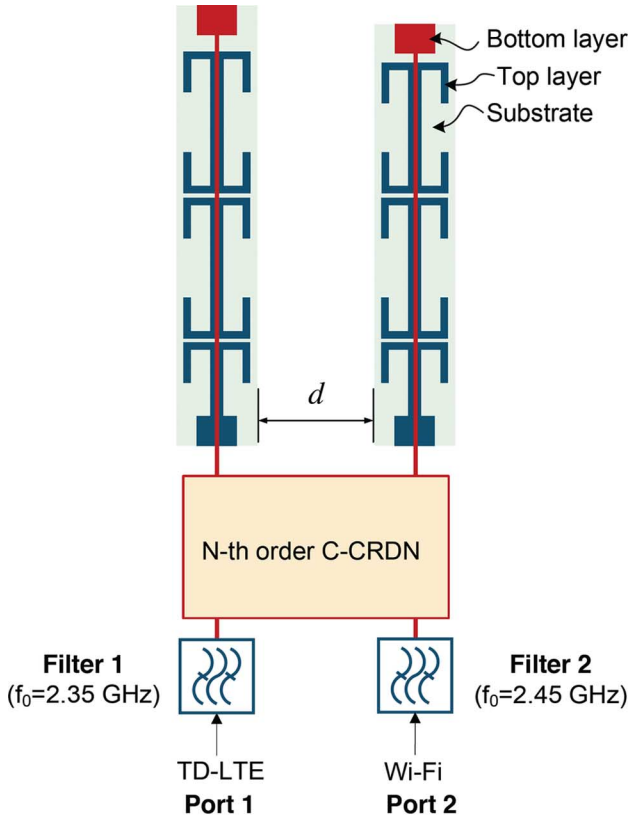

Fig. 4. Connection diagram of coupled antennas with a C-CRDN. (a) Theoretic pre-selection bandpass filters. (b) In measurement setup.

the antennas are placed 380 mm ($3.04\ \lambda_0$ at 2400 MHz) apart, less than 25-dB isolation is observed. For a typical TD-LTE femto cell, whose transmitting power is around 20 ~ 23 dBm [18], the unwanted power that is coupled to its neighbor Wi-Fi system can be far above the receiver sensitivity level that is

around $-90 \sim -70$ dBm, even with a $60 \sim 80$ dB filter rejection. Moreover, for TD-LTE band 40 and 2.4-GHz Wi-Fi systems, the frequency bands are contiguous, the isolation between them near the adjacent band edge are most difficult to deal with using conventional means. To demonstrate the C-CRDN device using the testing array shown in Fig. 4, two C-CRDNs with different orders are designed, fabricated, and tuned. Each design starts with the optimization of the coupled resonator circuit model given in Fig. 3 by minimizing the cost functions in (15). It should be noted that in the optimization process, the lengths of two transmission lines θ_1 and θ_2 shown in Fig. 3(a) are preset, but their values affect the resultant coupling coefficients since they affect the admittance matrix $[Y^A]$ of the coupled antennas.

Having had the optimum coupling coefficients obtained, a C-CRDN can be realized using coaxial combline resonators, which is similar to conventional filter realization, except that a C-CRDN is a *four-port* rather than a two-port device. Additionally, the design of a CRDN strongly depends on the S-parameters of the coupled antennas, therefore, the spacing between the antennas, as well as the surrounding environment, must be well controlled during the tuning and measurement process. The detailed design procedure and the performance comparison are given in Sections III-A–III-E.

A. Design of C-CRDNs by Optimization

At the initial stage, the high-gain antennas are fabricated using a Rogers Duroid printed circuit board (PCB) and placed on the test bench as shown Fig. 4(b). The scattering parameters of the coupled antennas are then measured by an Agilent N5227A network analyzer. It can be seen from Fig. 5(a) that the isolation between the two coupled antennas is not more than 25 dB within the frequency bands and that the matching performance in the two bands is not good either. Two fourth-order filters with one tri-section can be optimally design not only for rejecting the signal in the adjacent band, but also improving the matching condition. The designed coupling coefficients are listed in Table I (Filter 1–1 and 1–2), whose circuit models are inserted in the lower and higher channels, respectively, in order to obtain the responses shown in Fig. 5(a). It can be seen in Fig. 5(a) that the isolation between two antennas cannot be improved at the common boundary frequencies with the channel filters. Therefore, a C-CRDN needs to be designed to improve the isolation throughout the two adjacent bands.

In the design process, the coupling coefficients in (4) are the design variables to be optimized. The model in Fig. 3(a) are optimized by minimizing the cost functions in (15) using a gradient-based algorithm. The designed solutions of a fourth- and sixth-order C-CRDN for the given coupled sleeve antennas are listed in Table I, whose corresponding scattering parameters of the antennas cascaded by designed C-CRDNs are shown in Fig. 5(b) and (c), respectively.

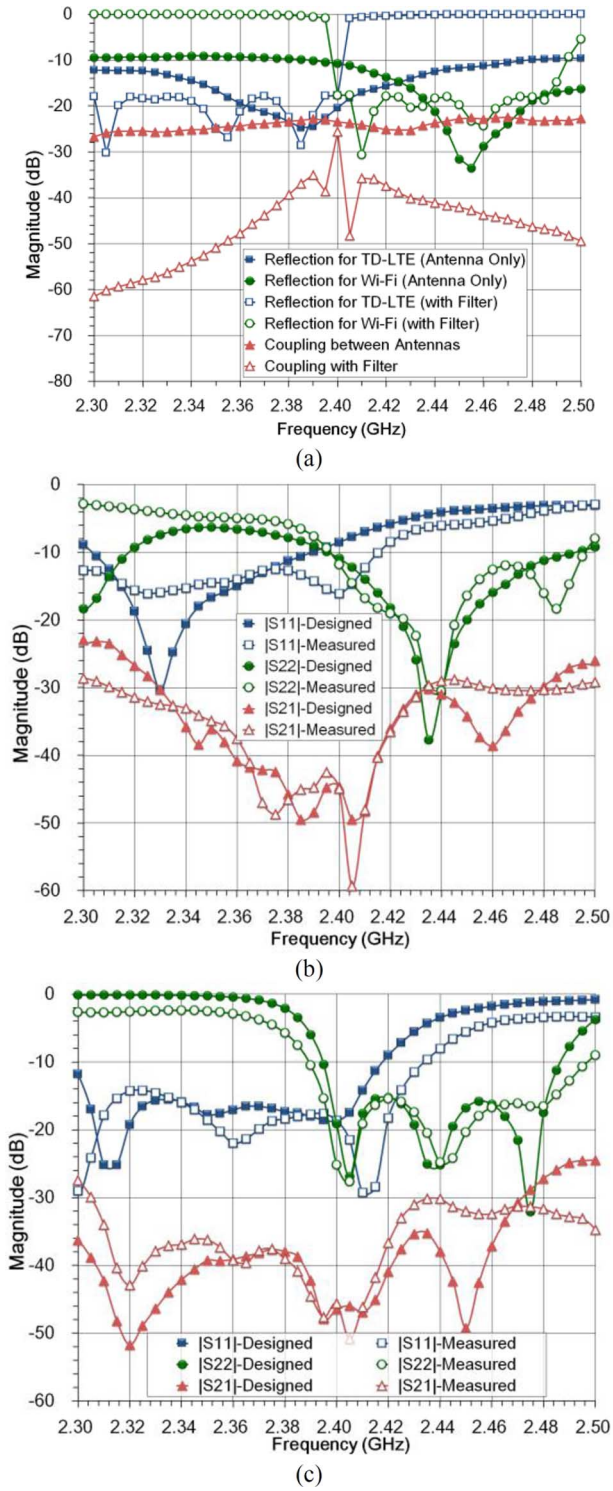

Fig. 5. Scattering parameters of the two coupled sleeve antennas: (a) with and without fourth-order filters, (b) with a designed fourth-order C-CRDN, and (c) with a designed sixth-order C-CRDN.

B. Parametric Study and Tuning Guidelines

To further reveal the effect of the design variables on the overall performance, the four cost functions in (15) are studied with respect to different combinations of the variables for the fourth-order C-CRDN example. In each parametric study, only one variable is swept while the other variables remain to be their optimized values, as given in Table II, and the routing diagram of a fourth-order C-CRDN is already given in Fig. 3(c). Some important observations are given as follows.

1) *The self-couplings:* The self-couplings of the two resonators next to the antenna ports will affect K_{11}, K_{22}, and K_{21}, while the self-couplings of the two resonators next to the transceivers only affect K_{11} and K_{22}.

TABLE I
COUPLING COEFFICIENTS OF FILTER1 AND FILTER2 (DESIGNED FBW = 4%)

Filter1-1 (For Antennas only)	m_{S1}	m_{12}	m_{23}	m_{34}	m_{4L}	m_{24}
	0.9351	0.8310	0.3417	0.4193	0.800	0.6184
	m_{11}	m_{22}	m_{33}	m_{44}	Q	f_0
	0.086	0.099	-0.852	-0.115	2950	2.35GHz
Filter1-2 (For Antennas only)	m_{S1}	m_{12}	m_{23}	m_{34}	m_{4L}	m_{24}
	0.8662	0.6716	0.2702	0.425	0.912	-0.649
	m_{11}	m_{22}	m_{33}	m_{44}	Q	f_0
	-0.065	-0.001	0.9102	0.000	2950	2.45GHz
Filter2-1 (4-th order CRDN)	m_{S1}	m_{12}	m_{23}	m_{34}	m_{4L}	m_{24}
	1.2496	1.1659	0.4578	0.5533	1.120	0.7932
	m_{11}	m_{22}	m_{33}	m_{44}	Q	f_0
	0.2320	0.2675	-0.838	0.3017	2950	2.35GHz
Filter2-2 (4-th order CRDN)	m_{S1}	m_{12}	m_{23}	m_{34}	m_{4L}	m_{24}
	1.4560	1.1961	0.5311	0.8040	1.3575	-0.9147
	m_{11}	m_{22}	m_{33}	m_{44}	Q	f_0
	0.000	0.000	0.9471	-0.137	2950	2.45GHz
Filter3-1 (6-th order CRDN)	m_{S1}	m_{12}	m_{23}	m_{34}	m_{4L}	m_{24}
	1.2467	1.1293	0.6022	0.6985	0.9646	0.5434
	m_{11}	m_{22}	m_{33}	m_{44}	Q	f_0
	0.0773	0.1515	-0.635	0.1908	2950	2.35GHz
Filter3-2 (6-th order CRDN)	m_{S1}	m_{12}	m_{23}	m_{34}	m_{4L}	m_{24}
	1.139	0.9605	0.4712	0.8336	1.3194	-0.8487
	m_{11}	m_{22}	m_{33}	m_{44}	Q	f_0
	-0.013	-0.105	0.9112	-0.004	2950	2.45GHz

TABLE II
COUPLING COEFFICIENTS OF DESIGNED AND MEASURE DC-CRDN FOR THE FOURTH-ORDER C-CRDN (DESIGNED FBW = 5%, F_0 = 2.4 GHz)

	Designed	Measured		Designed	Measured
$m_{P1\text{-}1}$	1.0640	1.0638	m_{12}	0.6546	0.6895
$m_{P2\text{-}2}$	1.6527	1.7124	m_{34}	2.3489	2.1330
$m_{P3\text{-}3}$	2.1955	2.1067	m_{11}	1.0998	0.8788
$m_{P4\text{-}4}$	1.5500	1.7452	m_{22}	-0.5985	-0.3498
m_{13}	2.8002	3.0000	m_{33}	1.5010	1.8164
m_{24}	2.7006	2.9974	m_{44}	-0.0279	-0.0825
θ_1		103°	θ_2		123°

2) *The I/O couplings:* The parametric study shows that K_{11} is independent of m_{P22} while K_{22} is independent of m_{P11}. Both m_{P11} and m_{P22} have the same effect on K_{21}. However, m_{P33} and m_{P44} are found to be related to K_{11}, K_{22}, and K_{21}.
3) *The main line couplings:* Similar to the I/O couplings, the main line coupling in the path to antenna 1 (m_{13}) will affect K_{22} a little and m_{24} will affect K_{11} very little.
4) *The cross couplings:* The cross coupling near the antennas, m_{34}, will affect K_{11}, K_{22}, and K_{21}, while the cross coupling near transceivers, m_{12}, will only affect K_{21}. These two couplings mainly control the isolation between the two channels. It is found that m_{12} can be tuned after m_{34} are tuned to its optimum value and the value of m_{12} are quite smaller than m_{34} in general.

The following helpful guideline for tuning a C-CRDN can be drawn from the above observations.

- m_{P33}, m_{P44}, and m_{34} must be tuned to the designed value in the first place: m_{P33} and m_{P44} are set to be large enough and m_{34} is mainly tuned to minimize K_{21}.
- The self-couplings in the path for the lower band signal must be positive while those for the higher band path must be negative.

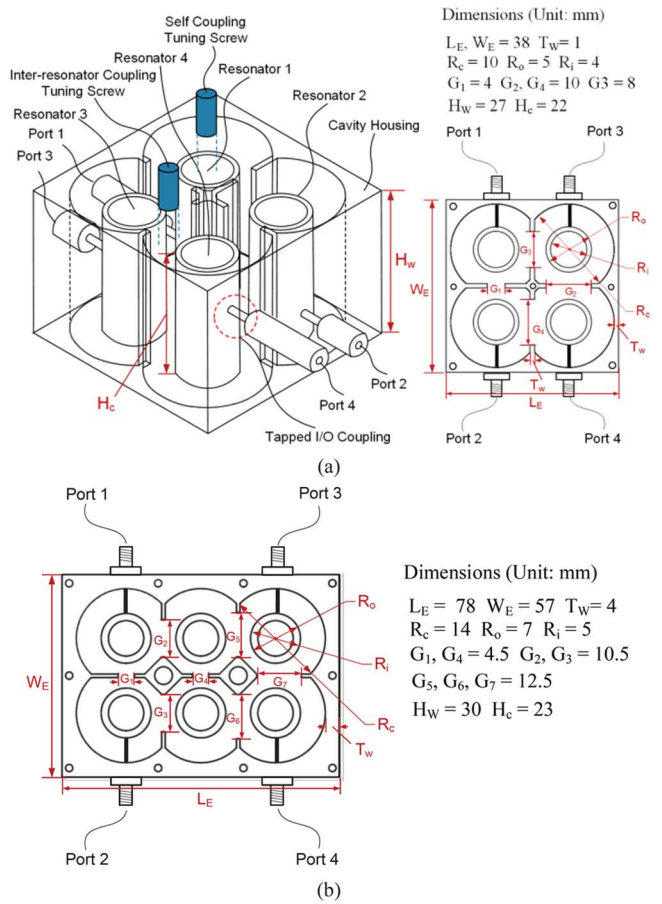

Fig. 6. (a) Sketch and dimensions of the fourth-order C-CRDN prototype and (b) sketch of the sixth-order C-CRDN; both of them are realized using coaxial combine resonators and M3 tuning screws.

TABLE III
COUPLING COEFFICIENTS OF DESIGNED AND MEASURED C-CRDN FOR THE SIXTH-ORDER C-CRDN (DESIGNED FBW = 5%, F_0 = 2.4 GHz)

	Designed	Measured		Designed	Measured
$m_{P1\text{-}1}$	0.9274	1.0405	m_{34}	1.8977	1.7370
$m_{P2\text{-}2}$	0.7704	0.8729	m_{56}	0.2471	0.3639
$m_{P3\text{-}3}$	1.8199	1.5606	m_{11}	0.7868	0.9239
$m_{P4\text{-}4}$	1.9996	1.8106	m_{22}	-0.7574	-0.9238
m_{15}	1.0271	1.2982	m_{33}	0.8116	0.7178
m_{35}	2.0318	2.0891	m_{44}	-0.6754	-0.8590
m_{26}	0.6935	0.8776	m_{55}	0.7868	0.9239
m_{46}	1.6680	1.7445	m_{66}	-0.7574	-0.9238
m_{12}	0.0000	0.0000			
θ_1		103°	θ_2		123°

- Since m_{13}, m_{P11}, and m_{11} will not affect K_{22}; m_{24}, m_{P22}, and m_{22} will not affect K_{11}, which suggests that the matching of the two ports can be independently tuned.
- m_{12} is tuned in the final step to further reduce K_{21}.

C. Realization and Tuning

Since the design of a C-CRDN strongly depends on the characteristics of the two coupled antennas, the four-port S-parameter matrix obtained by full-wave electromagnetic (EM) simulation of a C-CRDN with 50-Ω port reference impedance must be terminated by a complex two-port S-parameter matrix that

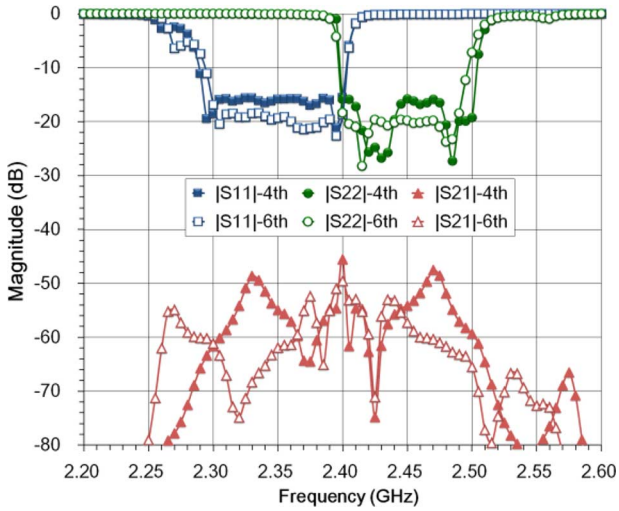

Fig. 7. Measured scattering parameters of the two coupled antennas with the fourth- or sixth-order C-CRDN prototype and theoretic channel filters.

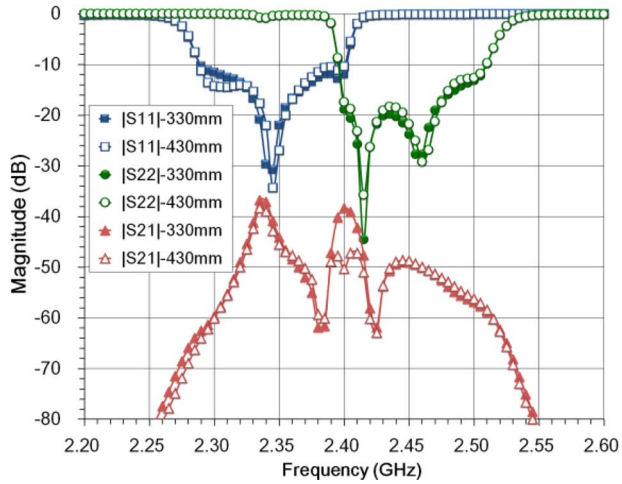

Fig. 8. Measured scattering parameters of the antennas decoupled by the sixth-order C-CRDN prototype with two spacing perturbation between two antennas.

describes the two coupled antennas at the antenna end. EM simulation software Agilent EMPro [19] is used in this study.

Two C-CRDN prototypes are designed, fabricated, and tuned. At each tuning stage, the corresponding parameters to the circuit model given in Fig. 3(a) are extracted from the measured responses using the Agilent ADS circuit simulator and optimization engine [20]. Compared to the designed circuit model, one can easily know what direction to tune at each tuning step. The realized coupling coefficients extracted at the final stage are also given in Tables II and III for comparison. The physical layouts and dimensions of the fourth- and sixth-order C-CRDNs are shown in Fig. 6.

Having had the two C-CRDN prototypes tuned with best effort, each of them is cascaded to the two coupled antennas, as illustrated in Fig. 4. The measured responses of the two-port cascaded system are also superimposed in Fig. 5(b) and (c). It can be seen that the improvement in isolation is better than 20 dB near the boundary frequency 2.4 GHz for both C-CRDNs, but the matching performance of the sixth-order C-CRDN is better than its fourth-order counterpart.

D. Combination of a C-CRDN With Two Channel Filters

To investigate the performance of the C-CRDN in practical radio systems, two simulated preselection bandpass filters working at the TD-LTE and the unlicensed bands, respectively, are synthesized and cascaded to the systems as illustrated in Fig. 4(a). Both theoretic filters are fourth order. The filter for TD-LTE band has been designed to have a transmission zero at 2.45 GHz, while the filter for the Wi-Fi band has a transmission zero at 2.35 GHz. Each transmission zero is realized by a tri-section coupling scheme. The S-parameters of the two decoupled channels by combing channel filters with the fourth- and sixth-order C-CRDNs are superposed in Fig. 7 with the synthesized couplings coefficients for the filters listed in Table I. It should be noted that since the matching conditions for the fourth- and sixth-order C-CRDNs are different, the synthesized filters for the two cases are different in order to match the different complex loads [21].

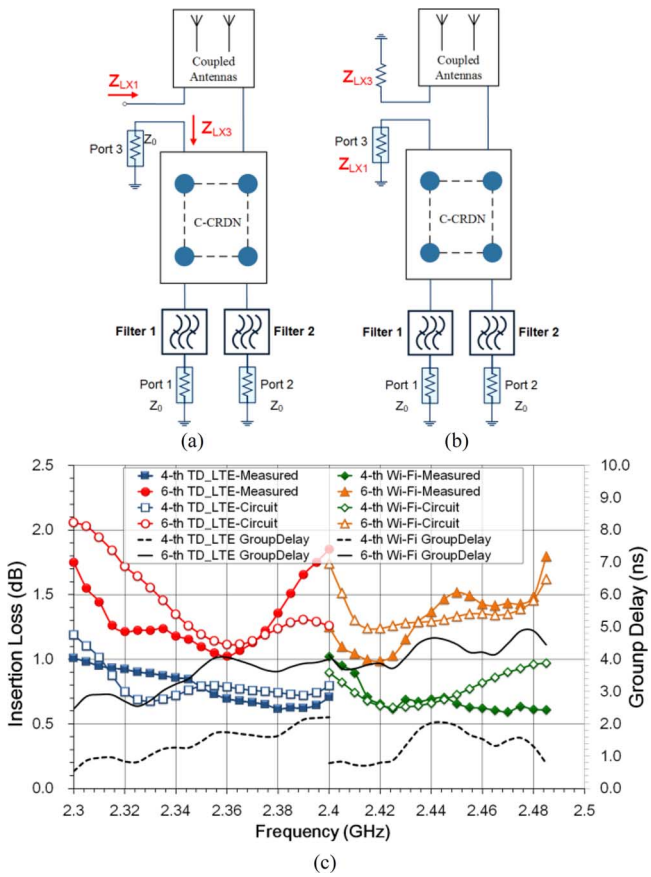

Fig. 9. Network model to extract the complex load looking into: (a) antenna 1 and (b) antenna 2. (c) Insertion losses and the measured group delays for the fourth- and sixth-order CRDNs in the two channels.

It is understandable that the performance of a C-CRDN depends on the characteristic of the coupled antennas. Therefore, the two-port responses of the sixth-order C-CRDN prototype when cascaded to the two coupled antennas with two spacing perturbations are superposed in Fig. 8. Deviations caused by $\pm 13\%$ spacing variance in both the reflection and isolation parameters are observed. Although the isolation property does not

change too much, the performance degradation in reflection coefficients is more obvious because of the change in the antenna matching condition.

E. Insertion Loss and Group Delay Introduced by a C-CRDN

To quantify the insertion loss introduced by a C-CRDN, the four-port S-parameters referenced to 50 Ω must be renormalized with appropriate loading effect. The network model shown in Fig. 9(a) is used to extract the complex load Z_{LX1} looking into the port of antenna 1 and the load Z_{LX3} looking into port 3 of a C-CRDN. The complex loads Z_{LX2} and Z_{LX4} looking into antenna 2 and port 4 of the C-CRDN, respectively, can also be extracted by the same token. With the network model illustrated in Fig. 9(b) with complex impedance Z_{LX1} and Z_{LX2} as port reference impedances at ports 3 and 4 of the C-CRDN, respectively, and 50-Ω impedance at the other two ports, the insertion losses between ports 1 and 3 and that between ports 2 and 4 can be obtained by renormalizing the measured S-parameters of the four-port C-CRDN prototypes. The measured insertion losses are shown in Fig. 9(c). For extracting the insertion loss of a CRDN when the network is matched, the channel filters are applied and are set to be lossless. Similarly, the measured group delays can also be obtained by the same circuit model and are plotted in Fig. 9(c). The unloaded Q for the fourth- and sixth-order C-CRDN prototypes are about 1200 and 1800, respectively. The simulated insertion losses with the unloaded Q's and the circuit model are also included in Fig. 9(c) for comparison. Similar to a coaxial combline filter, the insertion loss can be reduced by increasing unloaded Q of resonators.

IV. Concluding Remarks

The concept of the C-CRDN has been proposed in this paper for the first time. The concept has been proven by two hardware designs and prototypes for a realistic application scenario. Measurement results of the C-CRDN prototypes have demonstrated the effectiveness of the proposed new device in mitigating the interference between two collocated radio systems that work in adjacent frequency bands. It should be mentioned that the C-CRDN concept can also be applied to two radio systems operating in the same frequency band, thus supporting the applications of multiple-input multiple-output (MIMO) antenna systems, beam-forming systems, and full duplex radios.

Further development in this new device including higher order C-CRDNs with various coupling topologies as well as complete synthesis theory concerning multi-port multi-order C-CRDNs are under investigation.

References

[1] *Study on Signalling and Procedure for Interference Avoidance for In-Device Coexistence, V11.2.0*, 3GPP TR 36.816, Sep. 2011.

[2] Z. Hu, R. Susitaival, Z. Chen, I.-K. Fu, P. Dayal, and S. Baghel, "Interference avoidance for in-device coexistence in 3GPP LTE-advanced: Challenges and solutions," *IEEE Commun. Mag.*, vol. 50, no. 11, pp. 60–67, Nov. 2012.

[3] *Evolved Universal Terrestrial RadioAccess (LTE): Base Station (BS) Radio Transmission and Reception, ver. 10.2.0*, 3GPP TS 36.104, May 2011.

[4] W. F. Egan, *Practical RF System Design*. New York, NY, USA: Wiley, 2003.

[5] J. I. Choi, M. Jain, K. Srinivasan, P. Levis, and S. Katti, "Achieving single channel, full duplex wireless communication," in *Proc. 16th Annu. Int. Mobile Comput. Netw. Conf.*, 2010, pp. 1–12.

[6] A. Raghavan, E. Gebara, E. Tentzeris, and J. Laskar, "Analysis and design of an interference canceller for collocated radios," *IEEE Trans. Microw. Theory Techn.*, vol. 53, no. 11, pp. 3498–3508, Nov. 2005.

[7] H. Habibi, E. J. G. Janssen, R. G. M. Hilkens, Y. W. D. Milosevic, P. G. M. Baltus, and J. W. M. Bergmans, "Experimental evaluation of an adaptive nonlinear interference suppressor for multimode transceivers," *IEEE J. Emerg. Sel. Topics Circuits Syst.*, vol. 3, no. 4, pp. 602–614, Dec. 2013.

[8] C. Volmer, J. Weber, R. Stephan, K. Blau, and M. A. Hein, "An eigen-analysis of compact antenna arrays and its application to port decoupling," *IEEE Trans. Antennas Propag.*, vol. 56, no. 2, pp. 360–370, Feb. 2008.

[9] L. Zhao, L. K. Yeung, and K.-L. Wu, "A coupled resonator decoupling network for two-element compact antenna arrays in mobile terminals," *IEEE Trans. Antennas Propag.*, vol. 62, no. 5, pp. 2767–2776, May 2014.

[10] A. S. Konanur, K. Gosalia, S. H. Krishnamurthy, B. Hughes, and G. Lazzi, "Increasing wireless channel capacity through MIMO systems employing co-located antennas," *IEEE Trans. Microw. Theory Techn.*, vol. 53, pp. 1837–1844, Jun. 2005.

[11] F. Yang and Y. R. Samii, "Microstrip antennas integrated with electromagnetic bandgap EBG structures: A low mutual coupling design for array applications," *IEEE Trans. Antennas Propag.*, vol. 51, no. 10 , pp. 2936–2946, Oct. 2003.

[12] C. Y. Chiu, C. H. Cheng, R. D. Murch, and C. R. Rowell, "Reduction of mutual coupling between closely-packed antenna element," *IEEE Trans. Antennas Propag.*, vol. 55, no. 6, pp. 1732–1738, Jun. 2007.

[13] R. J. Cameron, C. M. Kudsia, and R. R. Mansour, *Microwave Filters for Communication systems*. New York, NY, USA: Wiley, 2007.

[14] A. Garcia-Lampérez, M. Salazar-Palma, and T. K. Sarkar, "Analytical synthesis of microwave multiport networks," in *IEEE MTT-S Int. Microw. Symp. Dig.*, 2004, pp. 455–458.

[15] G. Macchiarella and S. Tamiazzo, "Novel approach to the synthesis of microwave diplexers," *IEEE Trans. Microw. Theory Techn.*, vol. 54, no. 12, pp. 4281–4290, Dec. 2006.

[16] T. F. Skaik, M. J. Lancaster, and F. Huang, "Synthesis of multiple output coupled resonator circuits using coupling matrix optimization," *IET Microw., Antennas, Propag.*, vol. 5, no. 9, pp. 1081–1088, Jun. 2011.

[17] U. Rosenberg and S. Amari, "New power distribution (combination) method with frequency selective properties," in *EuMC2012 Workshop*, Amsterdam, The Netherlands, Oct. 2012, [CD ROM].

[18] D. Lopez-Perez, I. Guvenc, G. de la Roche, M. Kountouris, T. Q. S. Quek, and J. Zhang, "Enhanced intercell interference coordination challenges in heterogeneous networks," *IEEE Wireless Commun.*, vol. 18, no. 3, pp. 22–30, Jun. 2011.

[19] EMPro 3-D EM Simulation Software. ver. 2012.09, Agilent Technol., Santa Clara, CA, USA, 2012.

[20] Advanced Design System (ADS). ver. 2012.08, Agilent Technol., Santa Clara, CA, USA, 2012.

[21] H. Meng and K.-L. Wu, "Direct optimal synthesis of a microwave bandpass filter with general loading effect," *IEEE Trans. Microw. Theory Techn.*, vol. 61, no. 7, pp. 2566–2573, Jul. 2013.

Luyu Zhao (S'09–M'14) was born in Xi'an, China, in 1984. He received the B.Eng. degree from Xidian University, Xi'an, China in 2007, and is currently working toward the Ph.D. degree at The Chinese University of Hong Kong, Shatin, NT, Hong Kong.

From 2007 to 2009, he was with the National Key Laboratory of Antennas and Microwave Technology, Xidian University, as a Research Assistant, where he was involved in software and hardware development of RF identification (RFID) technologies. His current research interests include design and applications of multiple antenna systems for next-generation mobile communication systems, as well as innovative passive RF and microwave components, circuits and systems.

Mr. Zhao was the recipient of the Best Student Paper Award of the 2013 IEEE 14th Hong Kong Antennas and Propagation (AP)/Microwave Theory and Techniques (MTT) Postgraduate Conference.

Ke-Wei Qian was born in Chongqing, China, in 1981. He received M.Eng. and Ph.D. degrees from the University of Electronic Science and Technology of China, Chengdu, Sichuan, China, in 2006 and 2012, respectively.

From 2013 to 2014, he was with the Department of Electronic Engineering, The Chinese University of Hong Kong, Shatin, NT, Hong Kong, where he was involved in various low-temperature co-fired ceramic (LTCC) multichip-module (MCM) designs for next-generation mobile communication systems. His current research interests include design and application of microwave and millimeter-wave circuits and systems.

Ke-Li Wu (M'90–SM'96–F'11) received the B.S. and M.Eng. degrees from the Nanjing University of Science and Technology, Nanjing, China, in 1982 and 1985, respectively, and the Ph.D. degree from Laval University, Quebec, QC, Canada, in 1989.

From 1989 to 1993, he was with the Communications Research Laboratory, McMaster University, as a Research Engineer and a Group Manager. In March 1993, he joined the Corporate Research and Development Division, COM DEV International, where he was a Principal Member of Technical Staff. Since October 1999, he has been with The Chinese University of Hong Kong, Shatin, NT, Hong Kong, where he is a Professor and the Director of the Radiofrequency Radiation Research Laboratory (R3L). His current research interests include partial element equivalent circuit (PEEC) and derived physically expressive circuit (DPEC) electromagnetic (EM) modeling of high-speed circuits, RF and microwave passive circuits and systems, synthesis theory and practices of microwave filters, antennas for wireless terminals, LTCC-based multichip modules (MCMs), and RF identification (RFID) technologies.

Prof. Wu is a member of the IEEE MTT-8 Subcommittee (Filters and Passive Components). He has served as a Technical Program Committee (TPC) member for many prestigious international conferences including the IEEE Microwave Theory and Techniques Society (IEEE MTT-S) International Microwave Symposium (IMS). He was an associate editor for the IEEE TRANSACTIONS ON MICROWAVE THEORY AND TECHNIQUES SOCIETY (2006–2009). He was the recipient of the 1998 COM DEV Achievement Award for the development of exact EM design software of microwave filters and multiplexers and the Asia–Pacific Microwave Conference Prize (2008 and 2012, respectively).